

Probing small-scale cosmological fluctuations with the 21 cm forest: effects of neutrino mass, running spectral index and warm dark matter

Hayato Shimabukuro,¹ Kiyotomo Ichiki,² Susumu Inoue,^{3,4} and Shuichiro Yokoyama⁴

¹*Department of Physics, Graduate School of Science, Nagoya University, Aichi, 464-8602, Japan **

²*Kobayashi-Maskawa Institute for the Origin of Particles and the Universe, Nagoya University, Aichi, 464-8602, Japan*

³*Max-Planck-Institut für Physik, 80805 München, Germany*

⁴*Institute for Cosmic Ray Research, University of Tokyo, Kashiwa, Chiba, 277-8582, Japan*

(Dated: December 3, 2024)

Although the cosmological paradigm based on cold dark matter and adiabatic, nearly scale-invariant primordial fluctuations is consistent with a wide variety of existing observations, it has yet to be sufficiently tested on scales smaller than those of massive galaxies, and various alternatives have been proposed that differ significantly in the consequent small-scale power spectrum (SSPS) of large-scale structure. Here we show that a powerful probe of the SSPS at $k \gtrsim 10 \text{ Mpc}^{-1}$ can be provided by the 21 cm forest, that is, systems of narrow absorption lines due to intervening, cold neutral hydrogen in the spectra of high-redshift background radio sources in the cosmic reionization epoch. Such features are expected to be caused predominantly by collapsed gas in starless minihalos, whose mass function can be very sensitive to the SSPS. As specific examples, we consider the effects of neutrino mass, running spectral index (RSI) and warm dark matter (WDM) on the SSPS, and evaluate the expected distribution in optical depth of 21 cm absorbers out to different redshifts. Within the current constraints on quantities such as the sum of neutrino masses $\sum m_\nu$, running of the primordial spectral index $dn_s/d\ln k$ and WDM particle mass m_{WDM} , the statistics of the 21 cm forest manifest observationally significant differences that become larger at higher redshifts. In particular, it may be possible to probe the range of $m_{\text{WDM}} \gtrsim 10 \text{ keV}$ that may otherwise be inaccessible. Future observations of the 21 cm forest by the Square Kilometer Array may offer a unique and valuable probe of the SSPS, as long as radio sources such as quasars or Population III gamma-ray bursts with sufficient brightness and number exist at redshifts of $z \gtrsim 10 - 20$, and the astrophysical effects of reionization and heating can be discriminated.

PACS numbers: 98.70.Vc, 98.80.-k, 98.80.Es

I. INTRODUCTION

Over the last decades, cosmological observations have provided us with a wealth of information about the structure and evolution of the universe. Dedicated studies of anisotropies in the cosmic microwave background (CMB) by the *COBE*, *WMAP* and *Planck* satellites as well as ground-based telescopes have yielded increasingly precise information on the spectrum of cosmic density fluctuations on the largest scales [1–5]. Extensive surveys of galaxies and clusters of galaxies and their gravitational lensing effects have clarified the power-spectrum of large-scale structure (LSS) on somewhat smaller scales [6]. Finally, investigations of inhomogeneities in intergalactic hydrogen through the Lyman alpha forest have led to valuable constraints on the distribution of cosmic structure on the smallest scales to date [7].

Most current observations can be accommodated consistently by the concordance Λ CDM cosmological model, based on cold dark matter (CDM), a cosmological constant, and a power-law spectrum of adiabatic primordial density fluctuations that is nearly scale-invariant [8]. However, the Λ CDM model has yet to be sufficiently

tested against observations on scales much smaller than those corresponding to massive galaxies. The small-scale power spectrum (SSPS), that is, the power spectrum of large-scale structure on such scales, is of great interest from different perspectives, not only for cosmology but also for fundamental physics.

On the premise that the concordance Λ CDM cosmology is basically valid, one aspect of the SSPS that has received great attention is its role in constraining the mass of neutrinos [9, 10]. The existence of finite rest mass of neutrinos has been demonstrated by experiments probing solar and atmospheric neutrino oscillations, which are sensitive to the relative mass differences between different neutrino families. An important cosmological effect caused by light, massive neutrinos is the suppression of the matter power spectrum on scales smaller than the free streaming scale, which becomes stronger when the total mass of neutrinos is larger. In turn, various cosmological observations including the SSPS can provide valuable upper limits on the total mass of neutrinos. Current such limits on the sum of neutrino masses of all families is conservatively of order $\sum m_\nu \lesssim 1 \text{ eV}$. It is of great interest whether further observations can improve on them or even provide measurements of the neutrino mass.

Going somewhat beyond the simplest Λ CDM model, an interesting possibility is that the spectrum of primordial fluctuations is not a pure power-law but has a running spectral index (RSI), that is, a spectral index n_s that

*Electronic address: bukuro@nagoya-u.jp

is scale-dependent. Standard, single-field, slow-roll models of cosmological inflation in the early universe predict a nearly scale-invariant spectrum with $n_s \simeq 1$, where $n_s - 1$ and $dn_s/d\ln k$ are expected to be first and second order respectively in the small, slow-roll parameters. However, in some inflation models, relatively large RSI can be realized [11, 12]. Current cosmological observations indicate $n_s - 1 = O(0.01)$, consistent with standard, slow-roll inflation models. More extensive observations over a wider range of scales including the SSPS should lead to more precise constraints and help to discriminate among inflation models that are indistinguishable in terms of n_s alone.

Finally, as a more drastic alternative to CDM, warm dark matter (WDM) with particles masses in the keV range has been proposed on various grounds. The cosmological effect of WDM is characterized by its free streaming scale that depends on its mass m_{WDM} . Whereas above this scale, it behaves similarly with CDM and is indistinguishable from it, below this scale, it dramatically suppresses the power spectrum, resulting in much fewer dark matter halos on small scales compared to CDM. One specific particle physics candidate for WDM is sterile neutrinos, which are currently constrained to have a mass somewhere in the range $m_{\text{WDM}} \sim 1 - 50$ keV [13, 14]. Furthermore, WDM has also been motivated from an astrophysical viewpoint. Current observations indicate that the abundance of satellite galaxies around the Milky Way and in the Local Group is much lower than compared to the abundance of CDM subhalos on corresponding scales, the so-called “missing satellites problem” [15, 16]. Although the resolution may lie in astrophysical feedback effects that preferentially quench star formation in smaller systems, WDM can provide an intriguing alternative explanation by attributing the lack of satellite galaxies to the absence of the relevant dark halos in such cosmologies. Such an interpretation may favor a WDM mass in the range of a few keV [17] (see however [18]). Further observations of the SSPS can offer a critical test of WDM as a viable dark matter candidate.

In order to investigate the SSPS in greater depth and test Λ CDM and its alternatives, the most direct approach would be to observationally probe dark matter halos on scales much smaller than those of galaxies in the present universe. However, this is made difficult by the fact that the bulk of the intergalactic medium (IGM) has been fully ionized after completion of cosmic reionization at $z \sim 6$. In such circumstances, the gas in sufficiently small halos, in particular “minihalos” with masses $M \lesssim 10^8 M_\odot$ and virial temperature $T_{\text{vir}} \lesssim 10^4$ K, is expected to have been substantially photoevaporated [19]. Thus the only way to probe such halos in the present day may be via gravitational lensing effects [20] or possibly DM annihilation gamma rays [21], which are very challenging prospects.

On the other hand, an alternative avenue may open up by focusing on redshifts $z > 6$, before cosmic reionization and minihalo photoevaporation have proceeded

significantly. At such epochs, the cold, neutral gas associated with collapsed systems may be observable as a series of redshifted absorption features due to the 21 cm transition in the continuum spectrum of luminous background radio sources such as radio quasars or possibly gamma-ray bursts (GRBs). Dubbed the “21 cm forest” in analogy with the Lyman alpha forest, previous work has shown that the gas in minihalos can give rise to numerous, narrow absorption features that may be observable with future facilities such as the Square Kilometer Array (SKA), as long as sufficiently bright radio sources exist at the relevant redshifts [22–24]. The mass function of minihalos is dependent on the SSPS on scales $k \gtrsim 10$ Mpc^{-1} , much smaller than the smallest scales that are at present observationally accessible via the Lyman alpha forest. Therefore, future observations of the 21 cm forest can potentially provide a very sensitive probe of the SSPS, which in turn can provide valuable constraints or measurements of fundamental physics parameters such as the neutrino mass, the WDM particle mass or RSI of primordial fluctuations, the prospects of which are the main topic of this paper.

Note that minihalos themselves are unlikely to harbor appreciable star formation, as their virial temperatures are below the threshold for efficient gas cooling via atomic transitions. However, the 21 cm forest signal can also be significantly affected by external astrophysical effects, such as a background of UV photons or heating of the gas via X-rays or shocks, which are expected to become progressively more important as cosmic reionization proceeds. Indeed, the implications of such astrophysical feedback processes have been the main focus of studies on the 21 cm forest so far [22–29]. Since the consequences for the 21 cm forest of the SSPS beyond the standard Λ CDM cosmology is being discussed here for the first time, as an initial step, here we choose not to account for the complicating effects of a UV background or heating caused by astrophysical sources. Thus we are able to isolate and clarify the effects of modifications to the SSPS itself. The neglect of feedback effects would be more justifiable at higher redshifts, $z \gtrsim 20$, where the formation and evolution of stars and other objects are expected to be more limited.

We mention that the global signal of 21 cm emission from minihalos and/or the IGM at high redshifts (for reviews, see [30–32]) has been previously discussed as a potentially powerful probe of the SSPS [33, 34]. However, the major obstacle to such prospects is the huge level of foreground emission, several orders of magnitude brighter than the expected signal, that must be removed very efficiently in order to observe such emission [35]. In contrast, foregrounds are not a concern for observing the 21 cm forest, as long as sufficiently bright background radio sources exist.

This paper is organized as follows. In Section II, we describe our basic assumptions and formulation regarding the halo gas profile, spin temperature, optical depth and abundance of absorbers. Section III continues with

how we formulate the modifications to the SSPS caused by massive neutrinos, RSI and WDM, and also presents the corresponding expectations for the 21 cm forest, in comparison with the standard Λ CDM case. We end with discussions on the observability, various caveats, and a summary in Section IV.

For our baseline cosmological model, we adopt Λ CDM with the following parameters from the latest Planck data: $\Omega_m = 0.3175$, $\Omega_b h^2 = 0.12029$, $\Omega_\Lambda = 0.68$, $H_0 = 100h$ [km/s/Mpc], $h = 0.67$, $\sigma_8 = 0.834$, where $\Omega_m, \Omega_b, \Omega_\Lambda$ are the densities of cold dark matter, baryons, and cosmological constant, respectively, in units of the critical density, H_0 is the Hubble constant, and σ_8 is the variance of mass fluctuations averaged over a sphere with radius $8h^{-1}$ Mpc [3].

II. BASIC FORMULATION

For the most part, our basic formulation follows that given by Furlanetto [22, 24], with due modifications for our purposes.

A. Halo gas profile

We start with the description of the gas density profile in dark matter halos. We assume that the dark matter potential is described by the Navarro, Frenk & White (NFW) profile [36, 37], characterized by the concentration parameter $y = r_{\text{vir}}/r_s$, where r_s is the scaling radius, and the virial radius r_{vir} is given by [38]

$$r_{\text{vir}} = 0.784 \left(\frac{M}{10^8 h^{-1} M_\odot} \right)^{1/3} \left[\frac{\Omega_m}{\Omega_m^z} \frac{\Delta_c}{18\pi^2} \right]^{-1/3} \times \left(\frac{1+z}{10} \right)^{-1} h^{-1} [\text{kpc}], \quad (1)$$

where $\Delta_c = 18\pi^2 + 82d - 39d^2$ is the overdensity of halos collapsing at redshift z with $d = \Omega_m^z - 1$ and $\Omega_m^z = \Omega_m(1+z)^3/(\Omega_m(1+z)^3 + \Omega_\Lambda)$ [39]. Here we follow the N-body simulation results of Gao et al. [40] for halos at high-redshift and assume that y is inversely proportional to $(1+z)$.

Within the dark matter halo, the gas is assumed to be isothermal and in hydrostatic equilibrium, in which case its profile can be derived analytically [27, 41]. The gas density profile is given by

$$\ln \rho_g(r) = \ln \rho_{g0} - \frac{\mu m_p}{2k_B T_{\text{vir}}} [v_{\text{esc}}^2(0) - v_{\text{esc}}^2(r)], \quad (2)$$

where

$$T_{\text{vir}} = 1.32 \times 10^4 \left(\frac{\mu}{0.6} \right) \left(\frac{M}{10^8 h^{-1} M_\odot} \right)^{2/3} \times \left[\frac{\Omega_m}{\Omega_m^z} \frac{\Delta_c}{18\pi^2} \right]^{1/3} \left(\frac{1+z}{10} \right) [\text{K}] \quad (3)$$

is the virial temperature [38], ρ_{g0} is the central gas density, m_p is the proton mass, and $\mu = 1.22$ is the mean molecular weight of the gas. The gas escape velocity at radius r , $v_{\text{esc}}(r)$ is written as

$$v_{\text{esc}}^2(r) = 2 \int_r^\infty \frac{GM(r')}{r'^2} dr' = 2V_c^2 \frac{F(yx) + yx/(1+yx)}{xF(y)}, \quad (4)$$

where $x \equiv r/r_{\text{vir}}$ and $F(y) = \ln(1+y) - y/(1+y)$, and V_c is the circular velocity given by [38]

$$V_c^2 = \frac{GM}{r_{\text{vir}}} = 23.4 \left(\frac{M}{10^8 h^{-1} M_\odot} \right)^{1/3} \left[\frac{\Omega_m}{\Omega_m^z} \frac{\Delta_c}{18\pi^2} \right]^{1/6} \times \left(\frac{1+z}{10} \right)^{1/2} [\text{km/s}]. \quad (5)$$

The gas escape velocity reaches its maximum of $v_{\text{esc}}^2(0) = 2V_c^2 y/F(y)$ at the center of the halo. The central density ρ_{g0} is normalized by the cosmic value of Ω_b/Ω_m and given by

$$\rho_{g0}(z) = \frac{(\Delta_c/3)y^3 e^A}{\int_0^y (1+t)^{A/t} t^2 dt} \left(\frac{\Omega_b}{\Omega_m} \right) \bar{\rho}_m(z), \quad (6)$$

where $A = 3y/F(y)$ and $\bar{\rho}_m(z)$ is the mean total matter density at redshift z .

In this work, we consider only the gas within r_{vir} . We note that gas outside r_{vir} and accreting onto the halo can provide a significant additional contribution to the absorption signal, although it is difficult to model accurately [22, 27].

B. Spin temperature

The optical depth to 21 cm absorption is determined by the HI column density and the excitation state of the hyperfine transition of the HI atom, characterized by the spin temperature T_s . Most generally, T_s is determined by the following equation describing the balance between absorption/emission of CMB photons, collisions with other particles and scattering with UV photons [30]:

$$T_S^{-1} = \frac{T_\gamma^{-1} + x_c T_K^{-1} + x_\alpha T_C^{-1}}{1 + x_c + x_\alpha}. \quad (7)$$

Here, $T_\gamma = 2.73(1+z)$ is the CMB temperature at redshift z , T_K is the gas kinetic temperature, T_C is the effective color temperature of the UV radiation field, and x_c and x_α are the coupling coefficients for collisions with particles and UV photons, respectively.

As discussed in Section I, in this work we choose not to account for any UV radiation field in order to understand better how the 21cm forest is affected by modification to the SSPS itself. Hence the relevant equation simplifies

$$T_S^{-1} = \frac{T_\gamma^{-1} + x_c T_K^{-1}}{1 + x_c}. \quad (8)$$

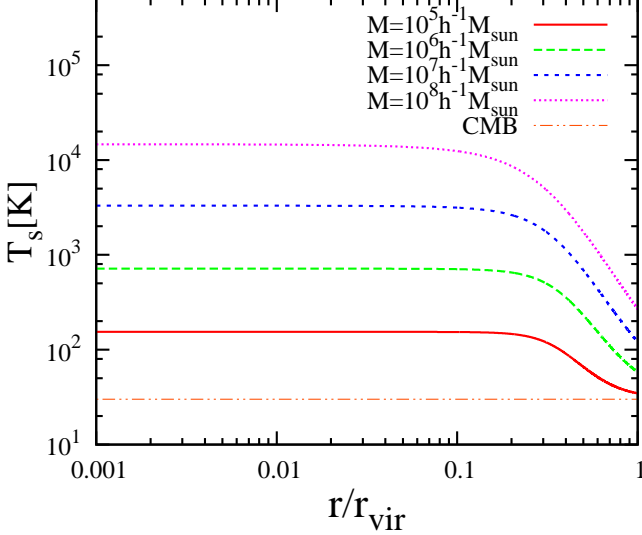


FIG. 1: Profiles of spin temperature for mini-halos at $z=10$ and different masses as indicated in the legend, versus radius normalized by the virial radius. The CMB temperature is shown by the horizontal line.

We also set $T_K = T_{\text{vir}}$, which should be a good approximation for mini-halos where gas cooling is inefficient. In principle, H_2 molecular cooling can reduce the gas temperature slightly below T_K [37] and increase the absorption optical depth, although this effect can be mitigated by H_2 destruction by a Lyman-Werner background [42].

The main contributions to collisional coupling are H-H and H- e^- collisions, and x_c is written as

$$x_c = x_c^{\text{HH}} + x_c^{\text{He}} = \frac{n_{\text{HI}} \kappa_{10}^{\text{HH}} T_*}{A_{10} T_\gamma} + \frac{n_e \kappa_{10}^{\text{eH}} T_*}{A_{10} T_\gamma}, \quad (9)$$

where n_{HI} is the number density of HI atoms, κ_{10}^{HH} and κ_{10}^{eH} are the de-excitation rates of H-H and H-e collisions, respectively, $A_{10} = 2.85 \times 10^{-15} \text{ s}^{-1}$ is the Einstein coefficient for the spontaneous decay of the 21 cm transition, and $T_* = 0.0682 \text{ K}$ is the equivalent temperature corresponding to the difference of the energy levels in the 21 cm transition. Since we do not account for the effects of cosmic reionization, the fraction of free electrons is small so that we can neglect the contribution from H-e collisions. The de-excitation rate κ^{HH} for $T_K \leq 300 \text{ K}$ is given by Zygelman [43]. For the temperature range of $T_K \geq 300 \text{ K}$, an approximate formula has been adopted in the literature [30].

The profiles of spin temperature for different mini-halo masses are shown in Fig.1. The spin temperature is equivalent to the virial temperature in the inner regions of mini-halos ($r \ll r_{\text{vir}}$), and decreases asymptotically to the CMB temperature toward the virial radius. This is due to the lower number density of the HI gas in the outer regions that makes collisional coupling less effective.

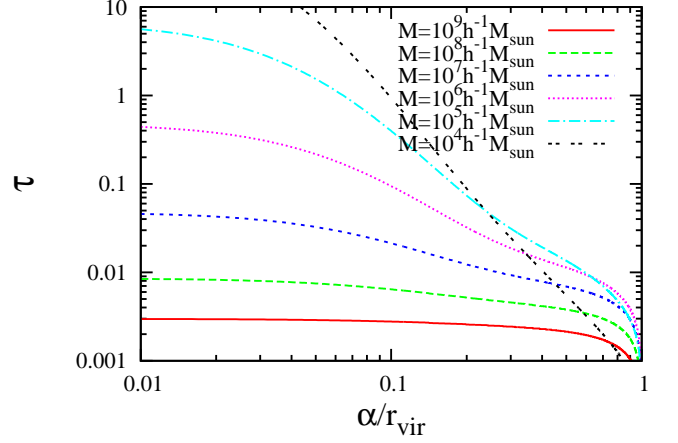


FIG. 2: Optical depths to 21 cm absorption for mini-halos at $z=10$ and different masses as indicated in the legend, as functions of the impact parameter normalized by the virial radius.

C. Optical depth

The optical depth to 21 cm absorption of a halo of mass M at impact parameter α at frequency ν can be written as an integral along the line of sight [22]:

$$\tau(\nu, M, \alpha) = \frac{3h_p c^3 A_{10}}{32\pi k_B \nu_{21}^2} \int_{-R_{\text{max}}(\alpha)}^{R_{\text{max}}(\alpha)} dR \frac{n_{\text{HI}}(r)}{T_S(r) \sqrt{\pi} b} \times \exp\left(-\frac{v^2(\nu)}{b^2}\right). \quad (10)$$

In Fig.2, the optical depths to 21 cm absorption for mini-halos of different masses at $z = 10$ are shown as a function of the impact parameter. Smaller impact parameters result in larger optical depths by virtue of the larger column density despite the higher spin temperature. We also note that mini-halos with smaller masses give larger optical depths when compared at the same impact parameter, which can be understood as follows. The halo mass dependence of the optical depth in Eq. (10) comes from n_{HI} , T_S and R_{max} . Roughly speaking, we can estimate $n_{\text{HI}} \sim M/r_{\text{vir}}^2$ and $T_S \sim T_{\text{vir}}$. As $r_{\text{vir}} \propto M^{1/3}$ and $T_{\text{vir}} \propto M^{2/3}$, we find $n_{\text{HI}} \propto M^{1/3}$ and $T_S \propto M^{2/3}$, pointing to larger optical depths for less massive halos. The actual dependence may be somewhat more complicated due to the non-trivial density profile. The width of the absorption feature is determined by $T_S \sim T_{\text{vir}}$ and expected to be of order a few kHz in observer frequency [22].

D. Abundance of absorbers

In order to evaluate the expected abundance of absorption features per redshift interval along an average line

of sight, we introduce a cumulative function

$$\frac{dN(>\tau)}{dz} = \frac{dr}{dz} \int_{M_{\min}}^{M_{\max}} dM \frac{dN}{dM} \pi r_{\tau}^2(M, \tau), \quad (11)$$

where dr/dz is the comoving line element, $r_{\tau}(M, \tau)$ is the maximum impact parameter in comoving units that gives optical depths greater than τ , and dN/dM is the halo mass function representing the comoving number density of collapsed dark matter halos with mass between M and $M + dM$, here given by the Press-Schechter formalism [44]. The maximum mass M_{\max} for minihalos is taken to correspond to $T_{\text{vir}} = 10^4$ K, below which gas cooling via atomic transitions and consequent star formation is expected to be inefficient. The minimum mass M_{\min} is assumed to be the Jeans mass determined by the IGM temperature [45],

$$M_J = \frac{4\pi\bar{\rho}}{3} \left(\frac{5\pi k_B T_{\text{IGM}}}{3G\bar{\rho}m_p\mu} \right)^{3/2} \simeq 3.58 \times 10^5 h^{-1} M_{\odot} \left(\frac{T_{\text{IGM}}}{1+z} \right)^{3/2} \quad (12)$$

where $\bar{\rho}$ is the total mass density including dark matter, and we choose $T_{\text{IGM}} = T_{\text{ad}}$, the average temperature of the IGM assuming only adiabatic cosmic expansion, consistent with our basic assumption of not accounting for astrophysical feedback effects.

III. NONSTANDARD COSMOLOGICAL EFFECTS AND RESULTS

Fig. 3 shows the abundance of 21 cm absorption features per redshift interval along an average line of sight as a function of optical depth at $z = 10$ and 20 for the baseline Λ CDM cosmology. Around a given z , the expected number of absorption features with a given τ is roughly $z\tau d^2N/dzd\tau$, which at $z = 10$ is seen to be $\sim 100, 5, 0.7$ for $\tau \sim 0.01, 0.1, 1$, respectively, appearing near observer frequency $\nu_{\text{obs}} \sim 129$ MHz. At $z = 20$, the numbers drop considerably, simply because structure formation is less advanced compared to $z = 10$, although one can still expect ~ 1 absorption feature with $\tau \sim 0.01$ at $\nu_{\text{obs}} \sim 68$ MHz.

Fig. 4 compares the contributions of different ranges of halo mass to the absorber abundance at $z = 10$ and $z = 20$, revealing that $M = 10^4 - 10^5 h^{-1} M_{\odot}$ is most important. With our assumption of M_{\min} as the Jeans mass for $T_{\text{IGM}} = T_{\text{ad}}$, $M_{\min} \sim 3.96 \times 10^4 h^{-1} M_{\odot}$ at $z=10$ and $M_{\min} \sim 1.68 \times 10^5 h^{-1} M_{\odot}$ at $z=20$, so the main contribution comes from minihalos with masses just above M_{\min} . On the other hand, minihalos with $M \sim 10^8 h^{-1} M_{\odot}$ hardly contribute to the absorbers for $\tau \gtrsim 0.01$, on account of their higher T_s as well as lower halo abundance.

In the following, we discuss how these baseline results are modified by the effects of neutrino mass, running spectral index and warm dark matter.

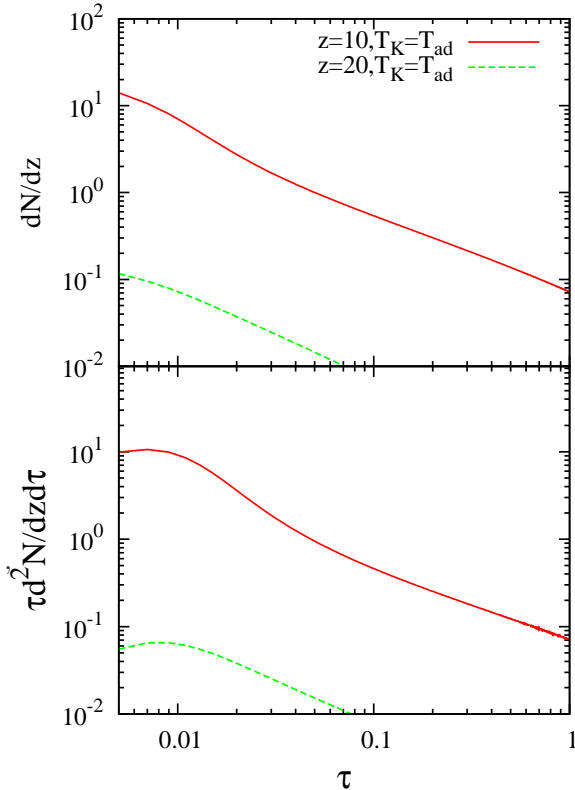


FIG. 3: *Top* : Abundance of 21 cm absorption features per redshift interval along an average line of sight at $z = 10$ (solid) and $z = 20$ (dashed) for the baseline Λ CDM cosmology. *Bottom* : Same as top panel, except in terms of the differential abundance per intervals in redshift and optical depth.

A. Neutrino mass

If neutrinos have mass, the evolution of neutrino perturbations after decoupling from the hot plasma in the relativistic regime is modified compared to the case with massless neutrinos. The Boltzmann equations that describe the evolution of the perturbations and the transfer function that relates initial conditions and density perturbations after recombination are changed accordingly [9]. In addition, the energy density ρ_m for massive neutrinos contribute as matter, as opposed to massless neutrinos that contribute as radiation. As a result, the matter power spectrum below the turnover scale and the corresponding halo mass function are suppressed compared to the massless case. In our calculation, we used the CAMB code for calculating the transfer function including massive neutrinos [46].

The free streaming scale of neutrinos with mass m_ν is given by [47]

$$k_{\text{fs}} \sim 0.026 \left(\frac{m_\nu}{\text{eV}} \right)^{1/2} \Omega_m^{1/2} h [\text{Mpc}^{-1}]. \quad (13)$$

The suppression of the matter power spectrum below the

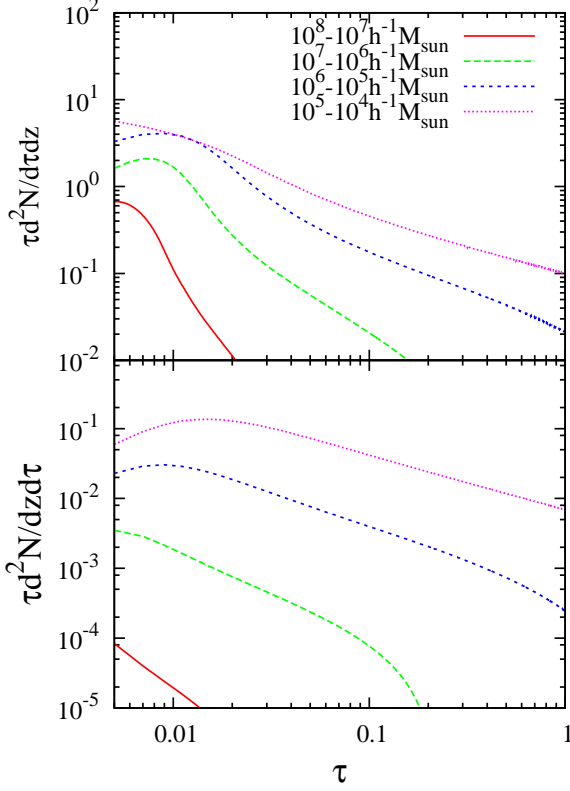


FIG. 4: Contribution of halos in different mass ranges to the abundance of 21 cm absorption features at $z=10$ (top) and $z=20$ (bottom).

free streaming scale is given by [47]

$$\left(\frac{\Delta P}{P}\right) \sim -8 \frac{\Omega_\nu}{\Omega_m} \sim -0.8 \left(\frac{m_\nu}{1\text{eV}}\right) \left(\frac{0.1N}{\Omega_m h^2}\right). \quad (14)$$

Here, N is the effective number of massive neutrino species, and Ω_ν is the energy density of massive neutrinos ρ_ν relative to the critical density ρ_{cr} ,

$$\Omega_\nu = \frac{\rho_\nu}{\rho_{cr}} = \frac{\sum_i m_i}{93.14 h^2 [\text{eV}]}, \quad (15)$$

where m_i is the mass of each neutrino family [9]. Taking all these into account, we plot the halo mass function including the effect of massive neutrinos in Fig.5. It can be seen that the suppression of the mass function is most prominent at the high mass end where it falls off exponentially.

Cosmological observations have already placed relatively tight constraints on neutrino masses. For example, upper bounds of $\sum m_\nu < 0.17$ eV and $\sum m_\nu < 0.26$ eV have been placed from observations of the Ly α forest and SDSS-III, respectively [10, 48], while recent *Planck* results give $\sum m_\nu < 0.66$ eV from the CMB alone [3]. To illustrate the effect of neutrino mass, we consider three cases, $\sum m_\nu = 0.1, 0.5$ and 1.0 eV.

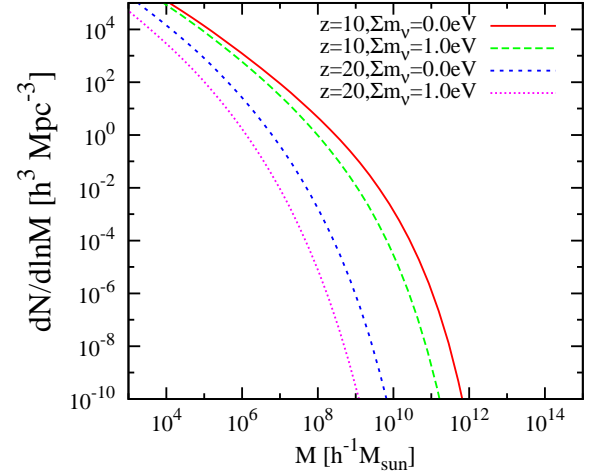


FIG. 5: Halo mass functions at $z=10$ and 20 for different values of the total mass of neutrinos as indicated in the legend.

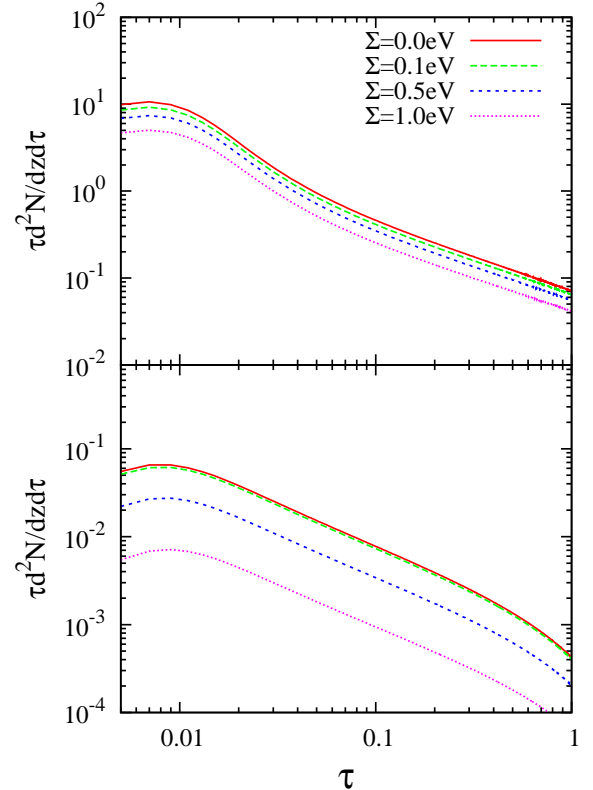


FIG. 6: Abundance of 21 cm absorption features per redshift interval at $z = 10$ (top) and $z = 20$ (bottom), for different values of the total neutrino mass $\sum m_\nu = 0.0\text{eV}, 0.1\text{eV}, 0.5\text{eV}$, and 1.0eV .

The abundance of absorbers for different neutrino masses at $z=10$ and 20 is shown in Fig.6. At $z=10$, the resulting differences are found to be quite small, less than a factor of 3 even for $\sum m_\nu = 1.0$ eV. However, at $z=20$, this can become much larger, reflecting the differences in the halo mass function in the mass range that is most important for the 21 cm forest signal, $M \approx 10^4 \sim 10^6 h^{-1} M_\odot$. Fig.5 shows that the exponential tail of the mass function, where the effect of the neutrino mass is largest, is much closer to this range for $z=20$ than for $z=10$. This is despite the fact that the suppression of the linear matter transfer function below the free streaming scale is actually smaller at higher redshifts [49].

At any rate, for the purpose of constraining neutrino masses, it is apparent that the 21 cm forest must be observed at $z \sim 20$ or higher in order to have any practical value in comparison with other methods. We return to this issue in Section IV.

B. Running spectral index

The running of the spectral index n_s of primordial fluctuations, $dn_s/d \ln k$, is defined by

$$\begin{aligned} \Delta_{\mathcal{R}}^2 &= \frac{k^3 \langle |\mathcal{R}_k|^2 \rangle}{2\pi^2} \\ &= \Delta_{\mathcal{R}}^2(k_0) \left(\frac{k}{k_0} \right)^{n_s - 1 + \frac{1}{2} \ln(k/k_0) dn_s/d \ln k}, \end{aligned} \quad (16)$$

where $k_0 = 0.05 \text{ Mpc}^{-1}$, and \mathcal{R}_k is the primordial curvature perturbation [50].

The latest constraints from Planck on the spectral index and RSI are $n_s = 0.9548 \pm 0.0073$ and $dn_s/d \ln k = -0.0149 \pm 0.0085$ in combination with WMAP polarization and high- l CMB data, and $n_s = 0.9596 \pm 0.0063$ and $dn_s/d \ln k = -0.0130 \pm 0.0090$ in combination with WMAP polarization and BAO data [51]. For several assumed combinations of the spectral index and RSI, we show the resulting halo mass function and abundance of 21 cm absorbers in Fig.7 and Fig.8, respectively.

In contrast to massive neutrinos that suppress the power spectrum uniformly at all scales below the free streaming scale, the effect of RSI can be potentially more significant, since it becomes progressively larger as one goes to smaller scales. However, taken into account the latest constraints from Planck and other observations, we see that its effect on the 21 cm forest at $z=10$ remains within a factor or a few. As with the case of massive neutrinos, the effect of RSI is found to be larger at $z=20$, for similar reasons: the most relevant range of halo masses for the 21 cm forest is closer to the high mass tail of the mass function, which is exponentially sensitive to changes in the fluctuation amplitude caused by RSI. Thus, if the 21 cm forest is observable at $z=20$ or higher, one may hope to obtain valuable constraints on RSI, which in turn

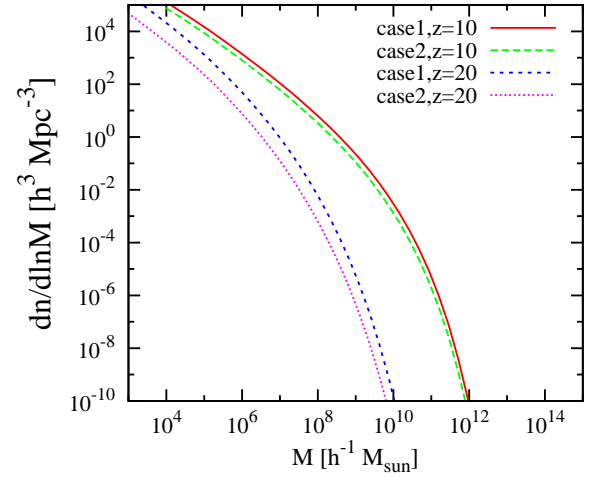


FIG. 7: Halo mass functions at $z=10, 20$ for various combinations of the spectral index and its running. Case1: $(n_s, dn_s/d \ln k) = (0.968, 0)$; case2: $(n_s, dn_s/d \ln k) = (0.9548, -0.0149)$.

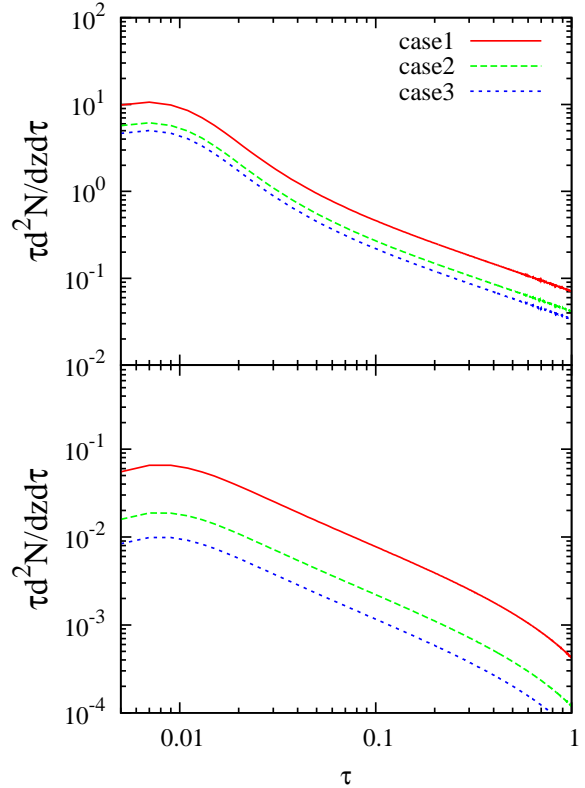


FIG. 8: Abundance of 21 cm absorption features per redshift interval at $z=10$ (top) and $z=20$ (bottom), for various combinations of the spectral index and its running. case1 : $(n_s, dn_s/d \ln k) = (0.968, 0)$, case2 : $(n_s, dn_s/d \ln k) = (0.9548, -0.0149)$ case3 : $(n_s, dn/d \ln k) = (0.96, -0.022)$. Note that case 2 corresponds to the constraints from Planck + WMAP polarization + high- l CMB data.

may help in discriminating different inflation models [11], independently from other observations.

C. Warm dark matter

To evaluate the halo mass function in the WDM cosmology, we utilize the prescription of Smith & Markovic [52]. For WDM of particle mass m_{WDM} and density Ω_{WDM} relative to the critical density, the comoving free streaming scale can be approximated by

$$\lambda_{\text{fs}} \sim 0.11 \left(\frac{\Omega_{\text{WDM}} h^2}{0.15} \right)^{1/3} \left(\frac{m_{\text{WDM}}}{\text{keV}} \right)^{-4/3} [\text{Mpc}]. \quad (17)$$

The mass scale below which halo formation is suppressed is [53]

$$M_{\text{fs}} = \frac{4}{3} \pi \left(\frac{\lambda_{\text{fs}}}{2} \right)^3 \bar{\rho}_m. \quad (18)$$

The halo mass function in the WDM cosmology is approximately [52]

$$\frac{dn}{dM}(M, z) = \frac{1}{2} \left\{ 1 + \text{erf} \left[\frac{\log_{10}(M/M_{\text{fs}})}{\sigma_{\log M}} \right] \right\} \left[\frac{dn}{dM} \right]_{\text{PS}}. \quad (19)$$

Here $\sigma_{\log M} = 0.5$, and $[dn/dM]_{\text{PS}}$ is the Press-Schechter mass function evaluated with a fitting formula for the matter power spectrum with WDM [54, 55]

$$P_{\text{WDM}}(k) = P_{\text{CDM}}(k) \{ [1 + (\alpha k)^{2\mu}]^{-5/\mu} \}^2, \quad (20)$$

where α and μ are fitting parameters given by

$$\alpha = 0.049 \left(\frac{m_{\text{WDM}}}{\text{keV}} \right)^{-1.11} \left(\frac{\Omega_{\text{WDM}}}{0.25} \right)^{0.15} \left(\frac{h}{0.7} \right)^{1.22} h^{-1} [\text{Mpc}] \quad (21)$$

and $\mu = 1.12$ [55].

The resulting halo mass functions at $z = 10$ and 20 for WDM with different particle masses compared with CDM are plotted in Fig.9. As can clearly be seen, WDM drastically suppresses the mass function below the mass scale M_{fs} that depends on m_{WDM} , while remaining identical to CDM above this scale.

Fig.10 shows the corresponding abundance of 21 cm absorbers for WDM, which manifest dramatic changes in accord with the halo mass function at small masses. The effects at $z = 20$ are even stronger than at $z = 10$, for reasons similar to that discussed above for neutrinos or RSI. In fact, if m_{WDM} is in the few keV range as is favored to explain the missing satellite problem [17], the suppression would be so great as to virtually make any 21 cm forest signal unobservable, as the relevant minihalos are much smaller than the satellites in question.

On the other hand, the cause of the missing satellite problem may lie in some kind of astrophysical feedback effect. From a particle physics perspective, WDM is still

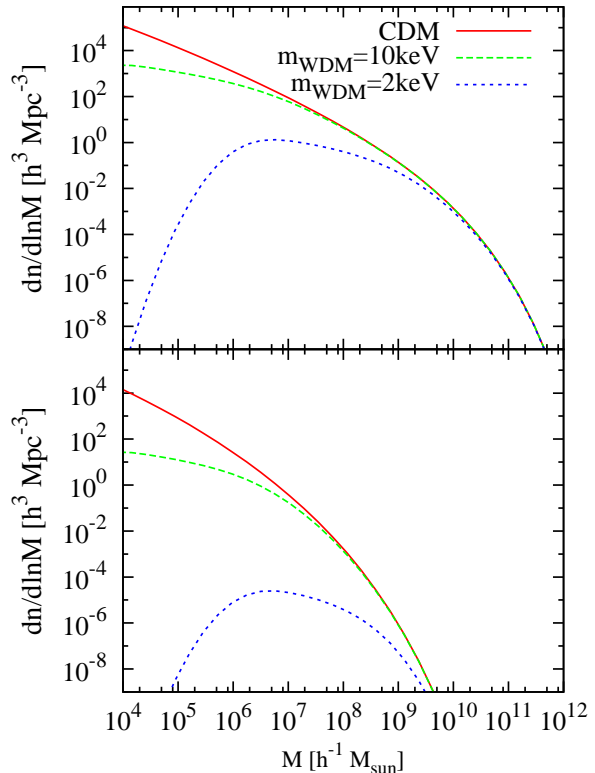


FIG. 9: Halo mass functions at $z = 10$ (top) and $z = 20$ (bottom) for CDM (red), and WDM with $m_{\text{WDM}} = 10$ keV (blue) and 2 keV (green).

motivated in some theories, for example as sterile neutrinos, whose mass has been constrained to be in the range ~ 1 -50 keV, also depending on the mixing angle (see Fig.2 in [13]). The current upper limits on their mass come from non-detections of X-ray lines caused by decaying sterile neutrinos in clusters of galaxies and the cosmic X-ray background. We see from Fig.10 that future observations of the 21 cm forest may provide an observable and potentially more sensitive probe of such particles with masses $m_{\text{WDM}} \gtrsim 10$ keV.

IV. DISCUSSION AND SUMMARY

We now turn to a discussion of the observability of the 21 cm forest due to minihalos. The principal question is the existence of background radio sources with sufficient brightness and number at the relevant frequency and redshifts of $z \sim 10 - 20$. The low temperatures of minihalos imply that the width of the expected absorption features are narrow, necessitating spectroscopy with frequency resolution of order $\Delta\nu \sim \text{kHz}$ at observer frequencies $\nu_{\text{obs}} \sim 70$ -130 MHz. Following [22], in order to detect absorption features of optical depth τ with frequency resolution $\Delta\nu$ and signal-to-noise S/N for an

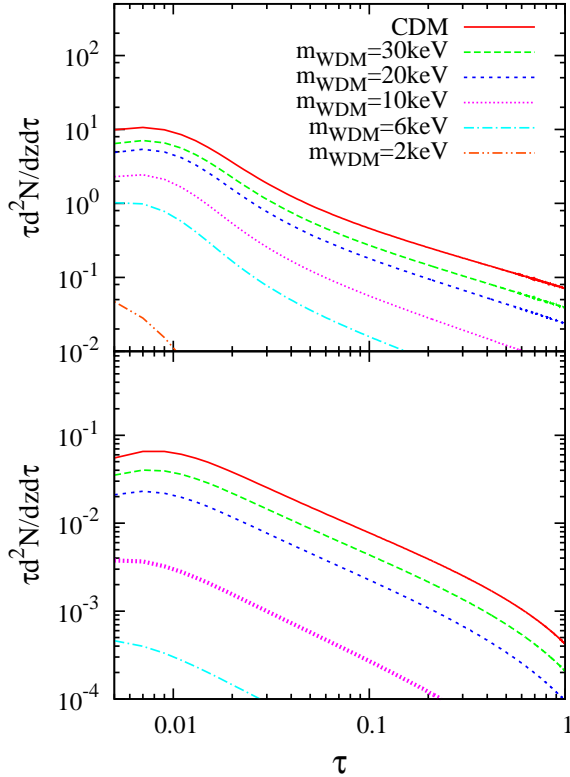


FIG. 10: Abundance of 21 cm absorption features per redshift interval at $z = 10$ (top) and $z = 20$ (bottom) for WDM with various particle masses as indicated in the legend.

integration time t_{int} , the required minimum background source brightness is

$$S_{\text{min}} = 16 \text{ mJy} \left(\frac{0.01}{\tau} \right) \left(\frac{S/N}{5} \right) \left(\frac{1 \text{ kHz}}{\Delta\nu} \right)^{1/2} \times \left(\frac{2.5 \times 10^3 [\text{m}^2/\text{K}]}{A_{\text{eff}}/T_{\text{sys}}} \right) \left(\frac{1 \text{ week}}{t_{\text{int}}} \right)^{1/2}, \quad (22)$$

where the specifications of SKA are adopted for the effective collecting area A_{eff} and system temperature T_{sys} .

Our results in Section III at face value show that spectroscopy of a single source with such properties at $z \sim 10$ may reveal tens to hundreds of absorption features with $\tau \sim 0.01 - 0.1$, which could already provide important information on the SSPS. Multiple sources would still be desirable to characterize fluctuations along different lines of sight. On the other hand, at $z \sim 10$, our neglect of astrophysical effects such as the UV background or reionization and heating of the IGM is hardly justifiable. As discussed below, in reality, such effects may completely dominate over any of the SSPS-related effects discussed above, which were quite small already at $z = 10$ except for WDM.

In this regard, $z \sim 20$ or higher would be much more preferable, since the formation of stars and galaxies and

their consequent feedback effects are likely to be considerably less advanced. Moreover, as seen in the previous section, the effects on the 21 cm forest caused by interesting non-standard physics aspects such as neutrino mass, running spectral index and warm dark matter all become significantly larger at $z \sim 20$. On the other hand, the expected number of absorption features is much less, only of order one with $\tau \sim 0.01$ along a given line of sight. Thus, at these redshifts, at least several (and preferably much more) background sources would be required for the 21 cm forest to be a useful probe of the SSPS.

Primary candidates for such sources at high redshifts are radio-loud quasars. For example, an object similar to a powerful, local radio galaxy such as Cyg A would have the requisite brightness if placed at $z \sim 10$ [23]. Estimates based on extrapolations of the observed radio luminosity functions to higher redshifts suggest that depending on the assumptions, there could be as many as $\sim 10^4 - 10^5$ and $\sim 10^3 - 10^4$ radio quasars with sufficient brightness in the whole sky at $z = 10$ and $z = 15$, respectively [25] (see also [56]). However, from a physical standpoint, it is an open question whether black holes with accordingly large masses could already have existed at such epochs.

An alternative possibility is the radio afterglows of certain types of GRBs. GRBs have already been observed up to $z \sim 8 - 9$, and it is plausible that they occur up to the earliest epochs of star formation in the universe at $z \sim 20$ or higher [57]. However, if such GRBs are similar to those seen at lower redshifts, their radio afterglows are not expected to be bright enough at the relevant observer frequencies $\nu_{\text{obs}} \sim 100$ MHz due to strong synchrotron self-absorption [58, 59]. On the other hand, it has been recently proposed that GRBs arising from Population (Pop) III stars forming in metal-free environments may be much more energetic compared to ordinary GRBs, which can generate much brighter low-frequency radio afterglows by virtue of their blastwaves expanding to larger radii over long timescales $t_{\text{rad, pk}} \sim 1000$ yr [60]. If the rate of Pop III GRBs with sufficiently bright radio emission is 0.1 yr^{-1} or roughly 10^{-4} of all GRBs, one can expect ~ 100 such sources all sky at a given time. Thus they may potentially suffice for 21 cm forest studies even at $z \sim 20$, albeit with large uncertainties. A practical question that remains is how we can observationally identify such sources. Further discussions on the observability of the 21 cm forest are beyond the scope of this paper and will be explored in future work.

Next, we briefly discuss some aspects of astrophysical feedback effects that we have chosen to neglect in this work in order to focus on the implications of the SSPS. Once the formation of stars and/or black holes is initiated in the universe, a background of UV and X-ray photons will build up over time. Ly α photons can resonantly scatter with hydrogen atoms and alter its hyperfine excitation state via the Wouthuysen-Field effect (see Eq.7) [30]. Furthermore, UV and X-ray photons as well as shocks driven by supernova explosions, quasar outflows,

etc. can heat the IGM to temperatures much above our assumed value of T_{ad} corresponding to simple, adiabatic cosmic expansion. The consequences of such effects on the 21 cm forest are likely to be significant [22–29], especially at $z \sim 10$, where it is clear that cosmic reionization is already in progress from CMB polarization measurements. As a simple illustration of such feedback effects, Fig.11 shows how the 21 cm forest at $z=10$ is affected by introducing a uniform temperature floor in the IGM at different values. The main consequence here is the increase of the Jeans mass, which eliminates the smaller minihalos that are predominantly responsible for the 21 cm forest signal and leads to its severe suppression. Compared to the effects of the SSPS discussed in Sec.III, those due to feedback exhibit a much stronger dependence on τ , which in principle may help in distinguishing the two. However, in practice, exploring the SSPS clearly favors observations at $z \sim 20$ and above where such feedback effects are expected to be more limited, in addition to the fact that the SSPS-related effects are larger, including those caused by massive neutrinos, running spectral index and warm dark matter.

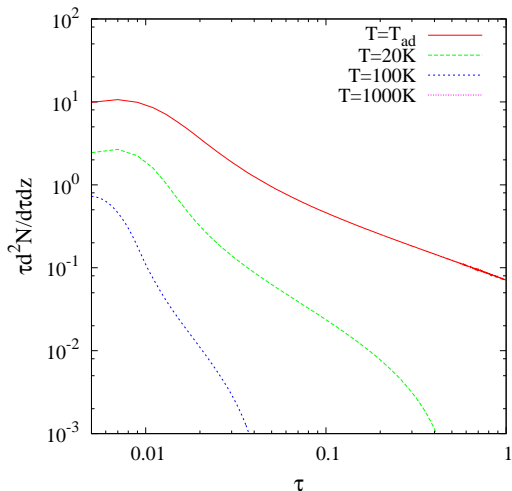


FIG. 11: Abundance of 21 cm absorption features per redshift interval at $z=10$ for different values of T_{IGM} as indicated in the legend.

To conclude, we have presented a novel approach to probe small-scale cosmological fluctuations utilizing the

21 cm forest, that is, absorption features caused by HI gas in minihalos in the spectrum of background radio sources at redshifts at $z \sim 10$ and above. The method is potentially sensitive to scales $k \gtrsim 10 \text{ Mpc}^{-1}$, much smaller than can be currently studied via observations of the CMB, galaxy clustering or the Ly α forest. New insight can be expected into aspects of physics beyond the standard Λ CDM cosmological model such as massive neutrinos, running of the primordial spectral index and warm dark matter. Radio quasars or Population III gamma-ray bursts are potential candidates for the background radio sources with the requisite brightness and number at the appropriate redshifts for future observations with SKA.

Of interest for further studies of the 21 cm forest that have not been considered here include uncertainties in the halo mass function at high redshifts [61–63], the effects of gas outside the virial radius accreting onto minihalos [22, 27], and the effects of relative streaming velocity between baryons and dark matter [64–66]. Further potentially interesting cosmological applications of the 21 cm forest include probes of primordial non-Gaussianity in relation to either the nonlinear, scale-dependent bias [67] or the halo mass function [68, 69], and probes of isocurvature primordial perturbations (e.g [70, 71]). We note that several recent papers have discussed the possibility of studying various aspects of the SSPS via the 21 cm emission signal [72–75], although efficient removal of the far brighter foreground emission poses a major observational challenge for realizing such prospects [35].

ACKNOWLEDGMENT

We would like to thank Keitaro Takahashi, Tsutomu T. Takeuchi, Kyungjin Ahn, Matt Jarvis, Takamitsu Tanaka and Eiichiro Komatsu for helpful comments and useful discussions. This work has been supported in part by Grant-in-Aid for Scientific Research Nos. 25-3015(HS), 24340048 (KI & SI), 24-2775 (SY) from the Ministry of Education, Sports, Science and Technology (MEXT) of Japan, and by Grant-in-Aid for the Global Center of Excellence program at Nagoya University “Quest for Fundamental Principles in the Universe: from Particles to the Solar System and the Cosmos” from the MEXT of Japan.

[1] G. F. Smoot, C. L. Bennett, A. Kogut, E. L. Wright, J. Aymon, N. W. Boggess, E. S. Cheng and G. De Amici *et al.*, *Astrophys. J.* **396**, L1 (1992).
[2] E. Komatsu *et al.* [WMAP Collaboration], *Astrophys. J. Suppl.* **192**, 18 (2011) [arXiv:1001.4538 [astro-ph.CO]].
[3] P. A. R. Ade *et al.* [Planck Collaboration], arXiv:1303.5076 [astro-ph.CO].
[4] J. L. Sievers *et al.* [Atacama Cosmology Telescope Collaboration], *JCAP* **1310**, 060 (2013) [arXiv:1301.0824

[astro-ph.CO]].
[5] Z. Hou, C. L. Reichardt, K. T. Story, B. Follin, R. Keisler, K. A. Aird, B. A. Benson and L. E. Bleem *et al.*, *Astrophys. J.* **782**, 74 (2014) [arXiv:1212.6267 [astro-ph.CO]].
[6] L. Anderson, E. Aubourg, S. Bailey, D. Bizyaev, M. Blanton, A. S. Bolton, J. Brinkmann and J. R. Brownstein *et al.*, *Mon. Not. Roy. Astron. Soc.* **427**, no. 4, 3435 (2013) [arXiv:1203.6594 [astro-ph.CO]].
[7] N. G. Busca, T. Delubac, J. Rich, S. Bailey, A. Font-

- Ribera, D. Kirkby, J. M. Le Goff and M. M. Pieri *et al.*, *Astron. Astrophys.* **552**, A96 (2013) [arXiv:1211.2616 [astro-ph.CO]].
- [8] J. P. Ostriker and P. J. Steinhardt, *Nature* **377**, 600 (1995).
- [9] J. Lesgourgues and S. Pastor, *Phys. Rept.* **429**, 307 (2006) [astro-ph/0603494].
- [10] K. N. Abazajian, E. Calabrese, A. Cooray, F. De Bernardis, S. Dodelson, A. Friedland, G. M. Fuller and S. Hannestad *et al.*, *Astropart. Phys.* **35**, 177 (2011) [arXiv:1103.5083 [astro-ph.CO]].
- [11] P. Adshead, R. Easther, J. Pritchard and A. Loeb, *JCAP* **1102**, 021 (2011) [arXiv:1007.3748 [astro-ph.CO]].
- [12] K. Kohri, Y. Oyama, T. Sekiguchi and T. Takahashi, *JCAP* **1310**, 065 (2013) [arXiv:1303.1688 [astro-ph.CO]].
- [13] A. Boyarsky, D. Iakubovskiy and O. Ruchayskiy, *Phys. Dark Univ.* **1**, 136 (2012) [arXiv:1306.4954 [astro-ph.CO]].
- [14] A. Kusenko, *Phys. Rept.* **481**, 1 (2009) [arXiv:0906.2968 [hep-ph]].
- [15] A. A. Klypin, A. V. Kravtsov, O. Valenzuela and F. Prada, *Astrophys. J.* **522**, 82 (1999) [astro-ph/9901240].
- [16] J. S. Bullock, arXiv:1009.4505 [astro-ph.CO].
- [17] E. Polisensky and M. Ricotti, *Phys. Rev. D* **83**, 043506 (2011) [arXiv:1004.1459 [astro-ph.CO]].
- [18] E. Polisensky and M. Ricotti, *Mon. Not. Roy. Astron. Soc.* **437**, 2922 (2014) [arXiv:1310.0430 [astro-ph.CO]].
- [19] P. R. Shapiro, I. T. Iliev and A. C. Raga, *Mon. Not. Roy. Astron. Soc.* **348**, 753 (2004) [astro-ph/0307266].
- [20] K. T. Inoue and C. Masashi, *Astrophys. J.* **633**, 23 (2005) [astro-ph/0503212].
- [21] M. Kuhlen, J. Diemand and P. Madau, *Astrophys. J.* **686**, 262 (2008) [arXiv:0805.4416 [astro-ph]].
- [22] S. Furlanetto and A. Loeb, *Astrophys. J.* **579**, 1 (2002) [astro-ph/0206308].
- [23] C. Carilli, N. Y. Gnedin and F. Owen, *Astrophys. J.* **577**, 22 (2002) [astro-ph/0205169].
- [24] S. Furlanetto, *Mon. Not. Roy. Astron. Soc.* **370**, 1867 (2006) [astro-ph/0604223].
- [25] Y. Xu, X. Chen, Z. Fan, H. Trac and R. Cen, *Astrophys. J.* **704**, 1396 (2009) [arXiv:0904.4254 [astro-ph.CO]].
- [26] A. Meiksin, *Mon. Not. Roy. Astron. Soc.* **417**, 1480 (2011) [arXiv:1102.1362 [astro-ph.CO]].
- [27] Y. Xu, A. Ferrara and X. Chen, *Mon. Not. Roy. Astron. Soc.* **410**, 2025 (2011) [arXiv:1009.1149 [astro-ph.CO]].
- [28] K. J. Mack and J. S. B. Wyithe, arXiv:1101.5431 [astro-ph.CO].
- [29] B. Ciardi, P. Labropoulos, A. Maselli, R. Thomas, S. Zaroubi, L. Graziani, J. S. Bolton and G. Bernardi *et al.*, arXiv:1209.2615 [astro-ph.CO].
- [30] S. Furlanetto, S. P. Oh and F. Briggs, *Phys. Rept.* **433**, 181 (2006) [astro-ph/0608032].
- [31] M. F. Morales and J. S. B. Wyithe, *Ann. Rev. Astron. Astrophys.* **48**, 127 (2010) [arXiv:0910.3010 [astro-ph.CO]].
- [32] J. R. Pritchard and A. Loeb, *Rept. Prog. Phys.* **75**, 086901 (2012) [arXiv:1109.6012 [astro-ph.CO]].
- [33] A. Loeb and M. Zaldarriaga, *Phys. Rev. Lett.* **92**, 211301 (2004) [astro-ph/0312134].
- [34] A. Loeb and S. Wyithe, *Phys. Rev. Lett.* **100**, 161301 (2008) [arXiv:0801.1677 [astro-ph]].
- [35] S. P. Oh and K. J. Mack, *Mon. Not. Roy. Astron. Soc.* **346**, 871 (2003) [astro-ph/0302099].
- [36] J. F. Navarro, C. S. Frenk and S. D. M. White, *Astrophys. J.* **490**, 493 (1997) [astro-ph/9611107].
- [37] T. Abel, G. L. Bryan and M. L. Norman, *Astron. Astrophys.* **540**, 39 (2000) [astro-ph/0002135].
- [38] R. Barkana and A. Loeb, *Phys. Rept.* **349**, 125 (2001) [astro-ph/0010468].
- [39] G. L. Bryan and M. L. Norman, *Astrophys. J.* **495**, 80 (1998) [astro-ph/9710107].
- [40] L. Gao, S. D. M. White, A. Jenkins, C. Frenk and V. Springel, *Mon. Not. Roy. Astron. Soc.* **363**, 379 (2005) [astro-ph/0503003].
- [41] N. Makino, S. Sasaki and Y. Suto, [astro-ph/9710344].
- [42] K. Ahn, P. R. Shapiro, I. T. Iliev, G. Mellema and U. -L. Pen, arXiv:0807.2254 [astro-ph].
- [43] Zygelman, B. 2005, *Astrophys. J.*, 622, 1356
- [44] W. H. Press and P. Schechter, *Astrophys. J.* **187**, 425 (1974).
- [45] P. Madau and M. Kuhlen, astro-ph/0303584.
- [46] A. Lewis, A. Challinor and A. Lasenby, *Astrophys. J.* **538**, 473 (2000) [astro-ph/9911177].
- [47] W. Hu, D. J. Eisenstein and M. Tegmark, *Phys. Rev. Lett.* **80**, 5255 (1998) [astro-ph/9712057].
- [48] R. de Putter, O. Mena, E. Giusarma, S. Ho, A. Cuesta, H. -J. Seo, A. J. Ross and M. White *et al.*, *Astrophys. J.* **761**, 12 (2012) [arXiv:1201.1909 [astro-ph.CO]].
- [49] K. Ichiki and M. Takada, *Phys. Rev. D* **85**, 063521 (2012) [arXiv:1108.4688 [astro-ph.CO]].
- [50] A. Kosowsky and M. S. Turner, *Phys. Rev. D* **52**, 1739 (1995) [astro-ph/9504071].
- [51] P. A. R. Ade *et al.* [Planck Collaboration], arXiv:1303.5082 [astro-ph.CO].
- [52] R. E. Smith and K. Markovic, *Phys. Rev. D* **84**, 063507 (2011) [arXiv:1103.2134 [astro-ph.CO]].
- [53] V. Avila-Reese, P. Colin, O. Valenzuela, E. D’Onghia and C. Firmani, *Astrophys. J.* **559**, 516 (2001) [astro-ph/0010525].
- [54] P. Bode, J. P. Ostriker and N. Turok, *Astrophys. J.* **556**, 93 (2001) [astro-ph/0010389].
- [55] M. Viel, J. Lesgourgues, M. G. Haehnelt, S. Matarrese and A. Riotto, *Phys. Rev. D* **71**, 063534 (2005) [astro-ph/0501562].
- [56] Z. Haiman, E. Quataert and G. C. Bower, *Astrophys. J.* **612**, 698 (2004) [astro-ph/0403104].
- [57] V. Bromm and A. Loeb, arXiv:0706.2445 [astro-ph].
- [58] S. Inoue, K. Omukai and B. Ciardi, *Mon. Not. Roy. Astron. Soc.* **380**, 1715 (2007) [astro-ph/0502218].
- [59] K. Ioka and P. Meszaros, *Astrophys. J.* **619**, 684 (2005) [astro-ph/0408487].
- [60] K. Toma, T. Sakamoto and P. Meszaros, *Astrophys. J.* **731**, 127 (2011) [arXiv:1008.1269 [astro-ph.CO]].
- [61] D. Reed, R. Bower, C. Frenk, A. Jenkins and T. Theuns, *Mon. Not. Roy. Astron. Soc.* **374**, 2 (2007) [astro-ph/0607150].
- [62] T. H. Greif, J. L. Johnson, R. S. Klessen and V. Bromm, arXiv:0803.2237 [astro-ph].
- [63] J. Bovy and C. Dvorkin, *Astrophys. J.* **768**, 70 (2013) [arXiv:1205.2083 [astro-ph.CO]].
- [64] D. Tseliakhovich, R. Barkana and C. Hirata, arXiv:1012.2574 [astro-ph.CO].
- [65] D. Tseliakhovich and C. Hirata, *Phys. Rev. D* **82**, 083520 (2010) [arXiv:1005.2416 [astro-ph.CO]].
- [66] A. Fialkov, R. Barkana, D. Tseliakhovich and C. M. Hirata, *Mon. Not. Roy. Astron. Soc.* **424**, 1335 (2012) [arXiv:1110.2111 [astro-ph.CO]].
- [67] S. Chongchitnan and J. Silk, arXiv:1205.6799 [astro-

- ph.CO].
- [68] S. Matarrese, L. Verde and R. Jimenez, *Astrophys. J.* **541**, 10 (2000) [astro-ph/0001366].
 - [69] M. LoVerde and K. M. Smith, *JCAP* **1108**, 003 (2011) [arXiv:1102.1439 [astro-ph.CO]].
 - [70] A. D. Linde and V. F. Mukhanov, *Phys. Rev. D* **56**, 535 (1997) [astro-ph/9610219].
 - [71] C. Gordon, D. Wands, B. A. Bassett and R. Maartens, *Phys. Rev. D* **63**, 023506 (2001) [astro-ph/0009131].
 - [72] Y. Oyama, A. Shimizu and K. Kohri, *Phys. Lett. B* **718**, 1186 (2013) [arXiv:1205.5223 [astro-ph.CO]].
 - [73] T. Sekiguchi and H. Tashiro, arXiv:1401.5563 [astro-ph.CO].
 - [74] T. Sekiguchi, H. Tashiro, J. Silk and N. Sugiyama, arXiv:1311.3294 [astro-ph.CO].
 - [75] Y. Takeuchi and S. Chongchitnan, arXiv:1311.2585 [astro-ph.CO].